

# Topological Data Analysis of Database Representations for Information Retrieval

Athanasios Vlontzos<sup>1,†</sup>, Yueqi Cao<sup>2</sup>, Luca Schmidtke<sup>1</sup>, Bernhard Kainz<sup>1</sup>, and Anthea Monod<sup>3</sup>

**1** Department of Computing, Imperial College London, UK

**2** Department of Mathematics, Beijing Institute of Technology, China

**3** Department of Mathematics, Imperial College London, UK

<sup>†</sup> Corresponding e-mail: athanasios.vlontzos14@imperial.ac.uk

## Abstract

Appropriately representing elements in a database so that queries may be accurately matched is a central task in information retrieval. This recently has been achieved by embedding the graphical structure of the database into a manifold so that the hierarchy is preserved. Persistent homology provides a rigorous characterization for the database topology in terms of both its hierarchy and connectivity structure. We compute persistent homology on a variety of datasets and show that some commonly used embeddings fail to preserve the connectivity. Moreover, we show that embeddings which successfully retain the database topology coincide in persistent homology. We introduce the dilation-invariant bottleneck distance to capture this effect, which addresses metric distortion on manifolds. We use it to show that distances between topology-preserving embeddings of databases are small.

**Keywords:** Bottleneck distance; Database embeddings; Information retrieval; Persistent homology; Poincaré ball.

## 1 Introduction

The fundamental problem of information retrieval (IR) is to find the most related elements in a database for a given query. Given that queries often comprise multiple components, candidate matches must satisfy multiple conditions, which gives rise to a natural hierarchy and connectivity structure of the database. This structure is important to maintain in performing IR. For example, when searching for a person named “John Smith” in a database, the search algorithm may search among all entries with the last name “Smith” and then among those entries, search for those with the first name “John.” Additionally, cycles and higher order topological features in the database correspond to entries that are directly related and may be, for instance, suitable alternative matches: as an example, in online shopping, when recommendations for other products are proposed as either alternative or complementary to the original query (i.e., they are recommended for their connection). The hierarchical and connectivity structure of databases motivates the study of the *topology* of databases. Topology characterizes abstract geometric properties of a set or space, such as its connectivity. Prior work has used point-set topology to describe databases (Egghe, 1998; Clementini et al., 1994; Egghe and Rousseau, 1998; Everett and Cater, 1992a). In this paper, we explore an alternative approach based on algebraic topology.

Topological data analysis (TDA) has recently been utilized in many fields and yielded prominent results, including imaging (Crawford et al., 2020; Perea and Carlsson, 2014), biology and neuroscience (Anderson et al., 2018; Aukerman et al., 2020), materials science (Hiraoka et al., 2016; Hirata et al., 2020), and sensor networks (Adams and Carlsson, 2015; de Silva and Ghrist, 2006). TDA has also recently gained interest in machine learning (ML) in many contexts, including loss function construction, generative adversarial networks, deep learning and deep neural networks, representation learning, kernel methods, and autoencoders (Brüel-Gabrielsson et al., 2019; Hofer et al., 2017, 2019; Hu et al., 2019; Moor et al., 2020; Reininghaus et al., 2015).

*Persistent homology* is a fundamental TDA methodology that extracts the topological features of a dataset in an interpretable, lower-dimensional representation (Edelsbrunner et al., 2000; Frosini and Landi, 1999; Zomorodian and Carlsson, 2005). Persistent homology is particularly amenable to data analysis since it

produces a multi-scale summary, known as a *persistence diagram*, which tracks the presence and evolution of topological features. Moreover, persistent homology is robust to noise and allows for customization of the chosen metric, making it applicable to a wide range of applications (Cohen-Steiner et al., 2007).

In this paper, we apply persistent homology to the setting of database queries and IR to understand the structure and connectivity of databases, which may be unknown, but may be summarized using topology. Persistent homology, in particular, provides an intuition on the prominence of each topological feature within the dataset. We show that the topological characteristics of a hierarchical and interdependent database structure are preserved in some commonly used embeddings and not in others. Moreover, we find that there is a high degree of similarity between topology-preserving embeddings. To capture and quantify this similarity, we introduce the *dilation-invariant bottleneck distance* for persistence diagrams to mitigate the issue of metric distortion in manifold embeddings. To the best of our knowledge, this is the first application of TDA to database representations.

**Related Work.** IR has been a topic of active research, particularly within the natural language processing (NLP) community. Document retrieval approaches have proposed a sequence-to-sequence model to increase performance in cross-lingual IR (Boudin et al., 2020; Liu et al., 2020). A particularly interesting challenge in IR in NLP is word-sense disambiguation, where the closest meaning of a word given a context is retrieved. Approaches to this problem have been proposed where the power of large language models is leveraged to embed not only words but also their contexts; the embeddings are further enriched with other sources, such as the WordNet hierarchical structure, before comparing the queries to database elements (Bevilacqua and Navigli, 2020; Scarlini et al., 2020; Yap et al., 2020). Inference is usually done either using cosine similarity as a distance function or through a learned network.

IR also arises in contexts other than NLP, such as image and video retrieval (Long et al., 2020). Image and video retrieval challenges, such as those proposed by Heilbron et al. (2015); Google (2018), have inspired the development of a wide variety of techniques.

*Topology-enabled IR.* Prior work that adapts topology to IR proposes topological analysis systems in the setting of point-set topology: these models are theoretical, and use separation axioms in topological spaces to describe the restriction on topologies to define a threshold for retrieval (Egghe, 1998; Clementini et al., 1994; Egghe and Rousseau, 1998; Everett and Cater, 1992b,a). A tool set based on point-set topology has also been proposed to improve the performance of enterprise-related document retrieval (Deolalikar, 2015).

## 2 Topological Data Analysis

TDA adapts algebraic topology to data. Classical topology studies features of spaces that are invariant under smooth transformations (e.g., “stretching” without “tearing”). A prominent example for such features is  $k$ -dimensional holes, where dimension 0 corresponds to connected components, dimension 1 to cycles, dimension 2 to voids, and so on. Homology is a theoretical concept that algebraically identifies and counts these features. The crux of topological data analysis is that topology captures meaningful aspects of the data, while algebraicity lends interpretability and computational feasibility.

### 2.1 Persistent Homology

Persistent homology adapts homology to data and outputs a set of topological descriptors that summarizes topological information of the dataset. Data may be very generally represented as a finite point cloud, which is a collection of points sampled from an unknown manifold, together with some similarity measure or metric. Point clouds may therefore be viewed as finite metric spaces. Persistent homology assigns a continuous, parameterized sequence of nested skeletal structures to the point cloud according to a user-specified proximity rule. The appearance and dissipation of holes in this sequence is tracked, providing a concise summary of the presence of homological features in the data at all resolutions. We now briefly formalize these technicalities; a complete discussion with full details can be found in the literature on applied and computational topology (e.g., Carlsson (2009); Ghrist (2008); Edelsbrunner and Harer (2008)).

Although the underlying idea of homology is intuitive, computing homology can be challenging. One convenient workaround is to study a discretization of the topological space as a union of simpler building blocks assembled in a combinatorial manner. When the building blocks are simplices (e.g., vertices, lines, triangles, and higher-dimensional facets), the skeletonized version of the space as a union of simplices is a simplicial complex, and the resulting homology theory is simplicial homology, for which there exist efficient computational algorithms (see, e.g., Munkres (2018) for a background reference on algebraic topology). Thus, in this paper, we will use simplicial homology over a field to study a finite topological space  $X$ ;  $(X, d_X)$  is therefore a finite metric space.

A  $k$ -*simplex* is the convex hull of  $k+1$  affinely independent points  $x_0, x_1, \dots, x_k$ , denoted by  $[x_0, x_1, \dots, x_k]$ ; a set of  $k$ -simplices forms a simplicial complex  $K$ . Simplicial homology is based on simplicial  $k$ -chains, which are linear combinations of  $k$ -simplices in finite  $K$  over a field  $\mathbb{F}$ . A set of  $k$ -chains thus defines a vector space  $C_k(K)$ .

**Definition 1.** The *boundary operator*  $\partial_k : C_k(K) \rightarrow C_{k-1}(K)$  maps to lower dimensions of the vector spaces by sending simplices  $[x_0, x_1, \dots, x_k] \mapsto \sum_{i=0}^k (-1)^i [x_0, \dots, \hat{x}_i, \dots, x_k]$  with linear extension, where  $\hat{x}_i$  indicates that the  $i$ th element is dropped.  $B_k(K) := \text{im } \partial_{k+1}$  is the set of *boundaries*;  $Z_k(K) := \ker \partial_k$  is the set of *cycles*. The  $k$ th *homology group* of  $K$  is the quotient group  $H_k(K) := Z_k(K)/B_k(K)$ .

Homology documents the structure of  $K$ , which is a finite simplicial complex representation of a topological space  $X$ . Simplicial complexes  $K$  may be constructed according to various assembly rules, which give rise to different complex types. In this paper, we work with the *Vietoris–Rips* (VR) complexes and filtrations.

**Definition 2.** Let  $(X, d_X)$  be a finite metric space, let  $r \in \mathbb{R}_{\geq 0}$ . The *Vietoris–Rips complex* of  $X$  is the simplicial complex with vertex set  $X$  where  $\{x_0, x_1, \dots, x_k\}$  spans a  $k$ -simplex if and only if the diameter  $d(x_i, x_j) \leq r$  for all  $0 \leq i, j \leq k$ .

A *filtration* of a finite simplicial complex  $K$  is a sequence of nested subcomplexes  $K_0 \subseteq K_1 \subseteq \dots \subseteq K_t = K$ ; a simplicial complex  $K$  that can be constructed from a filtration is a *filtered simplicial complex*. In this paper, filtrations are indexed by a continuous parameter  $r \in [0, t]$ ; setting the filtration parameter to be the diameter  $r$  of a VR complex yields the *Vietoris–Rips filtration*.

Persistent homology computes homology in a continuous manner when the simplicial complex evolves continuously over a filtration.

**Definition 3.** Let  $K$  be a filtered simplicial complex. The  $k$ th *persistence module derived in homology* of  $K$  is the collection  $\text{PH}_k(K) := \{H_k(K_r)\}_{0 \leq r \leq t}$ , together with associated linear maps  $\{\varphi_{r,s}\}_{0 \leq r < s \leq t}$  where  $\varphi_{r,s} : H_k(K_r) \rightarrow H_k(K_s)$  is induced by the inclusion  $K_r \hookrightarrow K_s$  for all  $r, s \in [0, t]$  where  $r \leq s$ .

Persistent homology, therefore, contains information not only on the individual spaces  $\{K_r\}$  but also on the mappings between every pair  $K_r$  and  $K_s$  where  $r \leq s$ . Persistent homology keeps track of the continuously evolving homology of  $X$  across all scales as topological features (captured by simplices) appear, evolve, and disappear as the filtered simplicial complex  $K$  evolves with the filtration parameter  $r$ .

Persistent homology outputs a collection of intervals where each interval represents a topological feature in the filtration; the left endpoint of the interval signifies when each feature appears (or is “born”), the right endpoint signifies when the feature disappears or merges with another feature (“dies”), and the length of the interval corresponds to the feature’s “persistence.” Each interval may be represented as a set of ordered pairs and plotted as a persistence diagram. A persistence diagram of a persistence module, therefore, is a multiset of points in  $\mathbb{R}^2$ . Typically, points located close to the diagonal in a persistence diagram are interpreted as topological “noise” while those located further away from the diagonal can be seen as “signal.” The distance from a point on the persistence diagram to its projection on the diagonal is a measure of the topological feature’s persistence. Figure 1 provides an illustrative depiction of a VR filtration and persistence diagram. In real data applications (and in this paper), persistence diagrams are finite.

## 2.2 Distances Between Persistence Diagrams

The set of all persistence diagrams can be endowed with various distance measures; under mild regularity conditions (of local finiteness of persistence diagrams), it is a rigorous metric space. The *bottleneck distance*

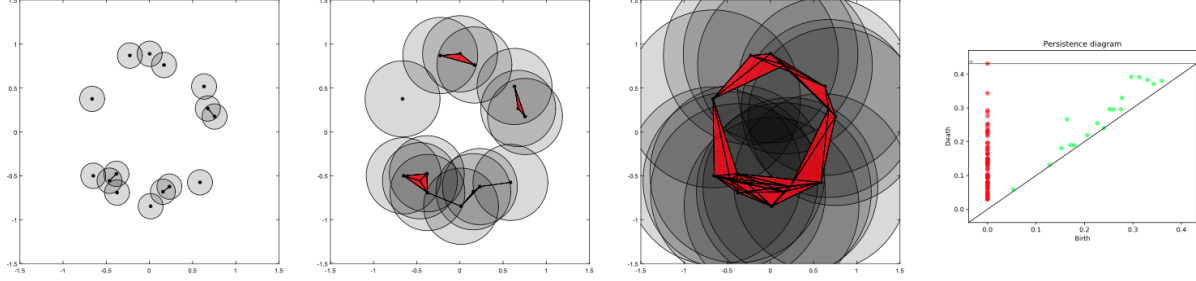


Figure 1: Illustration of a VR filtration and persistent homology. For a sample of points, a closed metric ball is grown around each point. The radius of the balls is the VR threshold,  $r$ . Points are connected by an edge whenever two balls have a non-empty intersection;  $k$ -simplices are spanned for intersections of  $k$  balls. As  $r$  grows, the collection of  $k$ -simplices evolves, yielding a VR filtration. The topology of the VR filtration is tracked in terms of the homological features (connected components, cycles, voids) that appear (are “born”), evolve, and disappear (“die”) as  $r$  grows, and documented in a persistence diagram (right-most). In this figure, red points correspond to  $H_0$  homology, or connected components, and green points correspond to  $H_1$  homology, or cycles.

measures distances between two persistence diagrams as a minimal matching between the two diagrams, allowing points to be matched with the diagonal  $\Delta$ , which is multiset of all  $(x, x) \in \mathbb{R}^2$  with infinite multiplicity, or the set of all zero-length intervals.

**Definition 4.** Let  $\mathcal{M}$  be the space of all finite metric spaces. Let  $\text{Dgm}(X, d_X)$  be the persistence diagram corresponding to the VR persistent homology of  $(X, d_X)$ . Let  $\mathcal{D} = \{\text{Dgm}(X, d_X) \mid (X, d_X) \in \mathcal{M}\}$  be the space of persistence diagrams of VR filtrations for finite metric spaces in  $\mathcal{M}$ . The *bottleneck distance* on  $\mathcal{D}$  is given by

$$d_\infty(\text{Dgm}(X, d_X), \text{Dgm}(Y, d_Y)) = \inf_{\gamma} \sup_{x \in \text{Dgm}(X, d_X)} \|x - \gamma(x)\|_\infty,$$

where  $\gamma$  is a multi-bijective matching of points between  $\text{Dgm}(X, d_X)$  and  $\text{Dgm}(Y, d_Y)$ .

The main stability theorem in persistent homology asserts that small perturbations in input data will result in small perturbations in persistence diagrams, measured by the bottleneck distance (Cohen-Steiner et al., 2007). This result together with its computational feasibility renders the bottleneck distance the canonical metric on the space of persistence diagrams for approximation studies in persistent homology.

Persistence diagrams, however, are not robust to the scaling of input data and metrics: the same point cloud measured by the same metric in different units results in different persistence diagrams with a potentially large bottleneck distance between them. One way that this discrepancy has been previously addressed is to study filtered complexes on a log scale, such as in Bobrowski et al. (2017); Buchet et al. (2016); Chazal et al. (2013). In these works, the persistence of a point in the persistence diagram (in terms of its distance to the diagonal) is based on the ratio of birth and death times, which alleviates the issue of artificial inflation in persistence arising from scaling. Nevertheless, log-scale persistence diagrams fail to recognize that two diagrams arising from the same input data measured by the same metric but in different units should coincide. The shift-invariant bottleneck distance addresses this issue by minimizing over all shifts along the diagonal, which provides scale invariance for persistence diagrams (Sheehy et al., 2018).

A further challenge is to recognize when the persistent homology of an input dataset is computed with two different metrics and we would like to deduce that the topology the dataset is robust to the choice of metric. Neither log-scale persistence nor the shift-invariant bottleneck distance is able to recognize when two persistence diagrams are computed from the same dataset but with different metrics. We therefore introduce the dilation-invariant bottleneck distance which mitigates this effect of metric distortion on persistence diagrams. The dilation-invariant bottleneck distance erases the effect of scaling between metrics used to construct the filtered simplicial complex and instead focuses on the topological structure of the point cloud.

**The Dilation-Invariant Bottleneck Distance.** Let  $(\mathcal{M}, d_{\text{GH}})$  be the space of finite metric spaces, equipped with Gromov–Hausdorff distance  $d_{\text{GH}}$ . Let  $\mathbb{R}_+$  be the multiplicative group on positive real numbers. Define the group action of  $\mathbb{R}_+$  on  $\mathcal{M}$  by

$$\begin{aligned} \mathbb{R}_+ \times \mathcal{M} &\rightarrow \mathcal{M}, \\ (c, (X, d_X)) &\mapsto (X, c \cdot d_X). \end{aligned} \tag{1}$$

The resulting quotient space  $\overline{\mathcal{M}} = \mathcal{M}/\mathbb{R}_+$  is a metric space with the *dilation-invariant Gromov–Hausdorff distance* defined by

$$\overline{d_{\text{GH}}}([X, d_X], [Y, d_Y]) = \inf_{c \in \mathbb{R}_+} d_{\text{GH}}((X, c \cdot d_X), (Y, d_Y)).$$

where  $[X, d_X]$  denotes the equivalence class in the quotient space. Our primary motivation for considering the above action is that multiplying a constant to the distance function results in a dilation on the persistence diagram. For VR persistence diagrams  $\text{Dgm}(X, d_X)$ , note that a simplex is in the VR complex of  $(X, d_X)$  with threshold  $r$  if and only if it is in the VR complex of  $(X, c \cdot d_X)$  with threshold  $cr$ . So any point in the persistence diagram  $\text{Dgm}(X, c \cdot d_X)$  is of the form  $(cu, cv)$  for some  $(u, v) \in \text{Dgm}(X, d_X)$ .

We can thus define an action following (1) that gives rise to a similar quotient space equipped with an appropriate metric between persistence diagrams that factors in dilation.

**Definition 5.** For the group action

$$\begin{aligned} \mathbb{R}_+ \times \mathcal{D} &\rightarrow \mathcal{D} \\ (c, \text{Dgm}(X, d_X)) &\mapsto \text{Dgm}(X, c \cdot d_X), \end{aligned}$$

we obtain the quotient space  $\overline{\mathcal{D}} = \mathcal{D}/\mathbb{R}_+$ , which may be endowed with the *dilation-invariant bottleneck distance* given by

$$\overline{d_{\infty}}(\text{Dgm}(X, d_X), \text{Dgm}(Y, d_Y)) = \inf_{c \in \mathbb{R}_+} d_{\infty}(\text{Dgm}(X, c \cdot d_X), \text{Dgm}(Y, d_Y)).$$

Let  $L : \mathcal{M} \rightarrow \mathcal{D}$  be the function sending each finite metric space to its VR-filtered persistence diagram, and  $\overline{L} : \overline{\mathcal{M}} \rightarrow \overline{\mathcal{D}}$  be the function between quotient spaces. We have the following commutative diagram.

$$\begin{array}{ccc} (\mathcal{M}, d_{\text{GH}}) & \longrightarrow & (\overline{\mathcal{M}}, \overline{d_{\text{GH}}}) \\ \downarrow L & & \downarrow \overline{L} \\ (\mathcal{D}, d_{\infty}) & \longrightarrow & (\overline{\mathcal{D}}, \overline{d_{\infty}}) \end{array}$$

**Theorem 6.** *The function  $\overline{L}$  is 1-Lipschitz.*

*Proof.* By Theorem 3.1 in Chazal et al. (2009), we have

$$d_{\infty}(\text{Dgm}(X, c \cdot d_X), \text{Dgm}(Y, d_Y)) \leq d_{\text{GH}}((X, c \cdot d_X), (Y, d_Y))$$

for any constant  $c \in \mathbb{R}_+$ . Taking the infimum on both sides with respect to  $c$  yields the conclusion.  $\square$

**Relation to the Shift-Invariant Bottleneck Distance.** We can use the above framework to obtain the shift-invariant bottleneck distance. The process is parallel to our construction of the dilation-invariant bottleneck distance.

Let  $\mathcal{F} = \{f : X \rightarrow \mathbb{R}\}$  be the space of continuous tame functions over a fixed triangulable topological space  $X$ , equipped with supremum metric  $d_{\mathcal{F}}(f, g) = \sup_x |f(x) - g(x)|$ . Define an isometric action of  $\mathbb{R}$  on  $\mathcal{F}$  by

$$\begin{aligned} \mathbb{R} \times \mathcal{F} &\rightarrow \mathcal{F} \\ (c, f) &\mapsto f + c. \end{aligned}$$

The resulting quotient space  $\overline{\mathcal{F}} = \mathcal{F}/\mathbb{R}$  is a metric space with the quotient metric defined by

$$\overline{d}_{\mathcal{F}}([f], [g]) = \inf_{c \in \mathbb{R}} \sup_{x \in X} |f(x) + c - g(x)| = \inf_{c \in \mathbb{R}} d_{\mathcal{F}}(f + c, g).$$

Let  $\mathcal{D}_{\infty} = \{\text{Dgm}(f) \mid f \in \mathcal{F}\}$  be the space of persistence diagrams of functions in  $\mathcal{F}$ , equipped with the standard bottleneck distance. Similarly, we can define the action

$$\begin{aligned} \mathbb{R} \times \mathcal{D}_{\infty} &\rightarrow \mathcal{D}_{\infty} \\ (c, \text{Dgm}(f)) &\mapsto \text{Dgm}(f + c) \end{aligned}$$

The resulting quotient space  $\overline{\mathcal{D}_{\infty}} = \mathcal{D}/\mathbb{R}$  is a metric space with the quotient metric define by

$$\overline{d}_{\infty}([\text{Dgm}(f)], [\text{Dgm}(g)]) = \inf_{c \in \mathbb{R}} d_{\infty}(\text{Dgm}(f + c), \text{Dgm}(g)).$$

Let  $S : \mathcal{F} \rightarrow \mathcal{D}_{\infty}$  be the function sending each tame function to its persistence diagram, and  $\overline{S} : \overline{\mathcal{F}} \rightarrow \overline{\mathcal{D}_{\infty}}$  be the function between quotient spaces. We have the following commutative diagram.

$$\begin{array}{ccc} (\mathcal{F}, d_{\mathcal{F}}) & \longrightarrow & (\overline{\mathcal{F}}, \overline{d}_{\mathcal{F}}) \\ \downarrow S & & \downarrow \overline{S} \\ (\mathcal{D}_{\infty}, d_{\infty}) & \longrightarrow & (\overline{\mathcal{D}_{\infty}}, \overline{d}_{\infty}) \end{array}$$

The function  $\overline{S}$  is also 1-Lipschitz, first by Cohen-Steiner et al. (2007),

$$d_{\infty}(\text{Dgm}(f + c), \text{Dgm}(g)) \leq d_{\mathcal{F}}(f + c, g)$$

and then taking the infimum on both sides with respect to  $c$ .

### 3 Implementation of Methods

In this section, we discuss the procedure of database representation in IR. We also describe our computation procedure for the dilation-invariant bottleneck distance.

#### 3.1 Database Representation for Information Retrieval: Manifold Embeddings

In this work, we apply persistent homology to study the database structures in their manifold-embedded representations rather than on the graphs themselves. Although persistent homology has been computed directly on graphs and networks (for instance, in applications in neuroscience (e.g., Patania et al., 2019)), manifolds may be equipped with a larger variety of metrics than graphs; moreover, on a manifold, distances may be defined between arbitration points along any path, while on a graph, we are constrained to traveling only along the graph edges. Since the metric is a fundamental component in computing persistent homology, it is desirable to work in a setting where we may study a variety of metrics in a computationally efficient manner to obtain a better understanding of the persistence structure of the databases.

In IR, a dataset  $Ds := \{d_1, \dots, d_N\}$  consisting of  $N$  data points is embedded in a latent manifold  $M$  via a model  $f$ . A query  $q$  is then embedded in the same space and compared against all or a subset of the elements of  $Ds$  via a distance metric  $d$ . The  $m$  closest matches are then returned. Formally, the returned set  $R_s$  is defined as  $R_s = \min_m \{d(f(Ds), f(q))\}$ . The local structure of the space as well as the global connectivity of the dataset  $Ds$  is of paramount importance in IR. Persistent homology is able to characterize both the global and local structure of the embedding space.

Following Nickel and Kiela (2017), we embed the hierarchical graph structure of our datasets onto a Euclidean manifold and a Poincaré ball by minimizing the loss function

$$\mathcal{L} = \sum_{(u,v) \in \mathcal{H}} \log \frac{e^{-d(u,v)}}{\sum_{v' \in \mathcal{N}(u)} e^{-d(u,v')}}, \quad (2)$$



where  $d$  is the distance of the manifold  $M$ ,  $\mathcal{H}$  is the set of hypernymity relations, and  $\mathcal{N} = \{v' \mid (u, v') \notin D\} \cup \{v\}$ , thus the set of negative examples of  $u$  including  $v$ .

In the case of the Euclidean manifold, we use two metrics: the standard  $L_2$  distance and the cosine similarity,

$$\text{sim}(x, y) = \frac{xy}{\|x\|\|y\|},$$

which has been used in inference in IR Scarlini et al. (2020); Yap et al. (2020). On the Poincaré ball, the distance is given by

$$d_P(x, y) = \cosh^{-1} \left( 1 + \frac{2\|x - y\|^2}{(1 - \|x\|^2)(1 - \|y\|^2)} \right), \quad (3)$$

where  $\|\cdot\|$  is the standard Euclidean norm. We optimize our model (2) directly on each of the manifolds with respect to these three metrics.

For the Poincaré ball, in addition to studying the direct optimization, we also study the representation of the Euclidean embedding on the Poincaré ball. The Euclidean embedding is mapped to the Poincaré ball using the exponential map (Mathieu et al., 2019):

$$\exp_x^c(z) = x \oplus_c \left[ \tanh \left( \frac{\sqrt{c} \lambda_x^c \|z\|}{2} \right) \frac{\hat{z}}{\sqrt{c}} \right],$$

where  $\hat{z} := z/\|z\|$ ,  $\lambda_x^c := 2/(1 - c\|x\|^2)$ , and  $\oplus_c$  denotes Möbius addition under the curvature  $c$  of the manifold (Ganea et al., 2018). Here, we take  $c = -1$ .

We calculate the VR persistent homology of the four embeddings to evaluate the current IR inference approaches from a topological perspective. Since we work with real-valued data, the maximum dimension for homology was set to 3. All persistent homology computations in this work were implemented using `giotto-tda` (Tausin et al., 2020). We note here that since VR persistent homology is computed, Ripser is available for very large datasets (Bauer, 2021). Ripser is currently the best-performing software for VR persistent homology computation both in terms of memory usage and wall-time seconds (3 wall-time seconds and 2 CPU seconds to compute persistent homology up to 2 dimensions of simplicial complexes of the order of  $4.5 \times 10^8$  run on a cluster, 3 wall-time seconds for the same dataset run on a shared memory system) (Otter et al., 2017).

### 3.2 Computing Dilation-Invariant Bottleneck Distances

We enumerate dilations in a suitable interval to approximate the dilation-invariant bottleneck distance. Specifically, let  $\text{Dgm}_1$  and  $\text{Dgm}_2$  be two persistence diagrams. Let  $\text{pers}(x) := \|x - \text{proj}_\Delta(x)\|$  be the persistence of a point  $x$  in a persistence diagram, where  $\text{proj}_\Delta(x)$  is the projection of  $x$  onto the diagonal  $\Delta$ . We compute the mean persistence as

$$\mu_{\text{Dgm}_i} = \frac{\sum_{x \in \text{Dgm}_i} \text{pers}(x)}{\#\{\text{off-diagonal points}\}},$$

and max persistence as  $M_{\text{Dgm}_i} = \max_{x \in \text{Dgm}_i} \text{pers}(x)$  for each diagram  $i = 1, 2$ . We then set  $\gamma_{\min}$  and  $\gamma_{\max}$  as

$$\gamma_{\min} = \min \left\{ \frac{M_{\text{Dgm}_2}}{M_{\text{Dgm}_1}}, \frac{\mu_{\text{Dgm}_2}}{\mu_{\text{Dgm}_1}} \right\},$$

$$\gamma_{\max} = \max \left\{ \frac{M_{\text{Dgm}_2}}{M_{\text{Dgm}_1}}, \frac{\mu_{\text{Dgm}_2}}{\mu_{\text{Dgm}_1}} \right\}.$$

The optimal dilation value  $r_k$  we want to search for lies in  $[c \cdot \gamma_{\max}, C \cdot \gamma_{\max}]$  where  $c \leq 1 \leq C$  are parameters that are manually set. For each  $r_k \in [c \cdot \gamma_{\min}, C \cdot \gamma_{\max}]$ , we compute the bottleneck distance  $d_\infty(r_k \cdot \text{Dgm}_1, \text{Dgm}_2)$ . The dilation-invariant bottleneck distance is approximated by the minimum among these bottleneck distances.

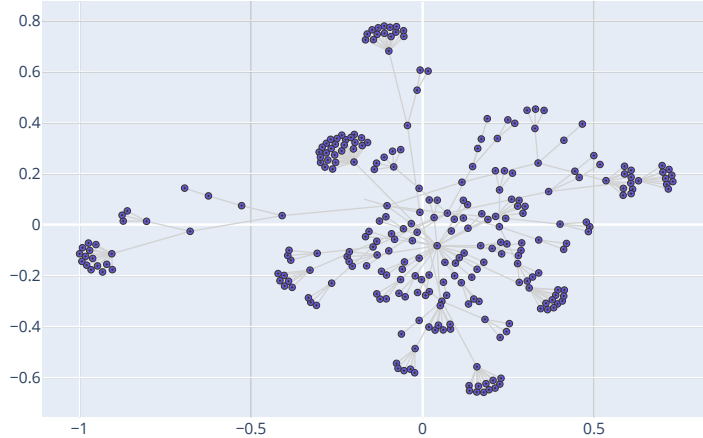


Figure 2: Visualization of ActivityNet Dataset. Note that hierarchical structure of the dataset naturally exhibits interesting topological properties such as cycles, clusters, and a tree-like structure.

## 4 Application to Data and Results

We evaluate our approach on two datasets that have a known hierarchical and network structure: the mammals closure of WordNet and ActivityNet.

**ActivityNet.** ActivityNet is an extensive labeled video dataset of 272 human actions that are accompanied by a hierarchical structure, visualized in Figure 2 (Heilbron et al., 2015). This dataset has been previously used in IR (Long et al., 2020).

**Mammals of WordNet.** WordNet is a lexical database that represents the hierarchy of the English language in a tree-like form, which has been extensively used in NLP (Miller, 1995). In our application, we focus on the subportion of WordNet relating to mammals. We pre-process this dataset by performing a transitive closure (Nickel and Kiela, 2017).

**Embedding the Data.** Both datasets were embedded in a 5-dimensional space, following Nickel and Kiela (2017). For both datasets, we trained the models for 1200 epochs with the default hyperparameters. For ActivityNet, we were able to achieve hypernimity mAP of 94.3% and 97.2% for the Euclidean manifold and Poincaré ball, respectively; while for the Mammals data, we achieved 45% and 82.3%, respectively. These results are consistent with Nickel and Kiela (2017).

### 4.1 Topology of the Euclidean Embeddings

The persistence diagrams of the Euclidean embeddings under both metrics and for both datasets are given in Figure 3. We see that up to scaling, the persistence diagrams for both embeddings into Euclidean space with respect to the  $L_2$  metric and cosine similarity are similar in terms of location and distribution of  $H_0$ ,  $H_1$ , and  $H_2$  points on the persistence diagrams. We quantify this similarity by computing dilation-invariant bottleneck distances. The graphs of the search procedure for each dataset are given in Figure 5. We first note that the standard bottleneck distances between the  $L_2$  and cosine similarity persistence diagrams are 1.642 for the ActivityNet dataset, and 0.6625 for the Mammals dataset. The dilation-invariant bottleneck distance is achieved at the minimum value of the bottleneck distance in our parameter search region. The dilation-invariant bottleneck distances between the  $L_2$  and cosine similarity persistence diagrams are 1.311 for the ActivityNet dataset and 0.4536 for the Mammals dataset.

The dilation parameter for Euclidean embeddings can be alternatively searched according to the scale of  $L_2$  embedded points as follows. Since mutual distances under the cosine embedding are always bounded by



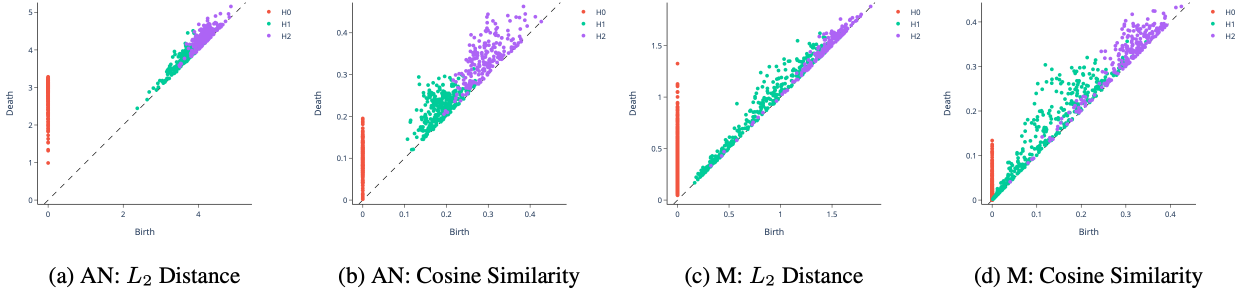


Figure 3: Persistence Diagrams of Euclidean Embeddings. AN: ActivityNet, M: Mammals.

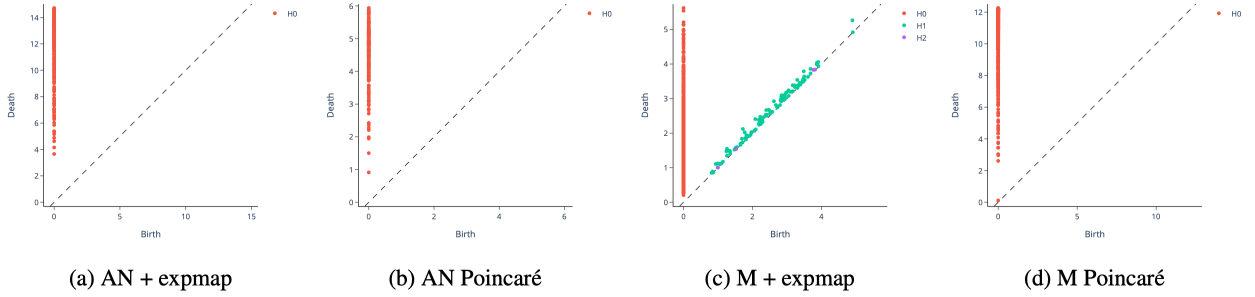


Figure 4: Persistence Diagrams of Poincaré Embeddings. AN: ActivityNet, M: Mammals, expmap signifies Euclidean optimization followed by an exponential map embedding into the Poincaré ball, while Poincaré signifies direct optimization on the Poincaré ball.

1, we can regard the induced finite metric space as a baseline. For the  $L_2$  embedding, mutual distances are affected by the scale of the embedded point cloud, i.e., if we multiply the points by a factor  $R$ , the induced metric will also dilate by a factor  $R$ . In experiments, the scale is 18.00 for the  $L_2$  embedding of ActivityNet and 6.588 for Mammals, which are consistent with dilation parameters we found.

The visual compatibility of the persistence diagrams together with the small dilation-invariant bottleneck distances indicate that the topology of the database is preserved in the Euclidean embedding, irrespective of the metric.

## 4.2 Topology of the Poincaré Ball Embeddings

The persistence diagrams for the Poincaré ball embeddings for both datasets are given in Figure 4. For the ActivityNet dataset, we see that both embeddings fail to identify the  $H_1$  and  $H_2$  homology inherent in the dataset (see Figure 2), which, by contrast, the Euclidean embeddings successfully capture. For the Mammals dataset, only the exponential map embedding into the Poincaré ball is able to identify  $H_1$  and  $H_2$  homology, but note that these are all points close to the diagonal. Their position on the diagonal indicates that the persistence of their corresponding topological features is not significant: these features are born and die almost immediately, are therefore likely to be topological noise. We now investigate this phenomenon further.

From (3), we note that an alternative representation for the distance function maybe obtained as follows. Set

$$A(x, y) := 1 + \frac{2\|x - y\|^2}{(1 - \|x\|^2)(1 - \|y\|^2)}, \quad (4)$$

then (3) may be rewritten as

$$d_P(x, y) = \log(A(x, y) + \sqrt{A(x, y)^2 - 1}). \quad (5)$$

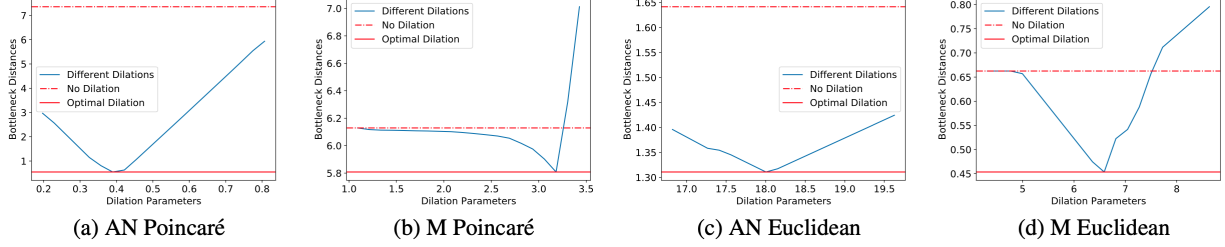


Figure 5: Dilation-Invariant Bottleneck Distances Between Embeddings. AN: ActivityNet, M: Mammals

We assume that  $\|x - y\|$  has a strictly positive lower bound and study the case when both points  $x, y$  lie near the boundary, i.e., both  $\|x\| \approx 1$  and  $\|y\| \approx 1$ . Notice, then, that (4) and (5) are approximated by

$$\begin{aligned}
 A(x, y) &\approx \frac{1}{2} \frac{\|x - y\|^2}{(1 - \|x\|)(1 - \|y\|)}, \\
 d_P(x, y) &\approx \log(2A(x, y)) \\
 &\approx 2\log(\|x - y\|) - \log(1 - \|x\|) - \log(1 - \|y\|).
 \end{aligned} \tag{6}$$

Notice also that

$$d_P(x, 0) \approx \log 2 - \log(1 - \|x\|). \tag{7}$$

Combining (6) and (7) yields the following approximation for the Poincaré distance:

$$d_P(x, y) \approx d_P(x, 0) + d_P(y, 0) + 2\log(\|x - y\|/2). \tag{8}$$

For points near the boundary, i.e.,  $d_P(x, 0) = R \gg 1$ , (8) gives a mutual distance of approximately  $2R$  between any given pair of points.

Recall from Definition 2 that a  $k$ -simplex is spanned if and only if the mutual distances between  $k + 1$  points are less than a given threshold  $r$ . The implication for discrete points near the boundary of the Poincaré ball is that either the threshold is less than  $2R$ , and then the VR complex is a set of 0-simplices; or the threshold is greater than  $2R$ , and then the VR complex is homeomorphic to a simplex in higher dimensions. That is, the VR filtration jumps from discrete points to a highly connected complex; this behavior is illustrated in Figure 6.

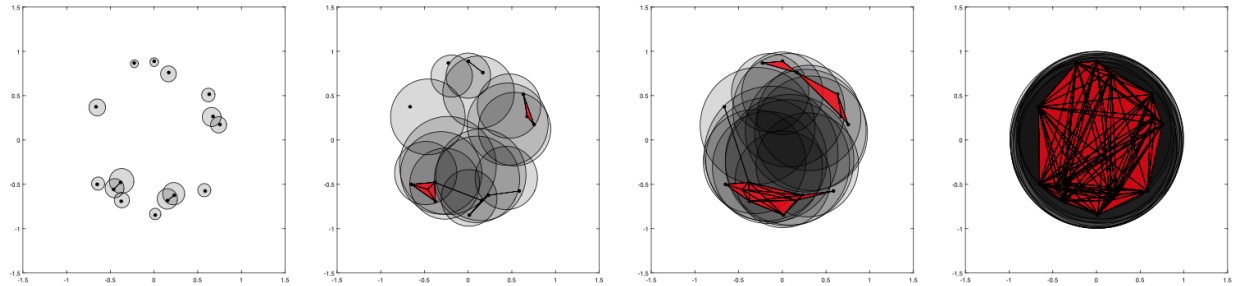


Figure 6: Illustration of connectivity behavior in a VR complex on the Poincaré ball equipped with the Poincaré distance. For points sampled near the boundary, the connectivity of the VR complex grows slowly at low threshold values (small radii) and quickly becomes highly connected as the threshold grows and we approach the approximation (8) for distances between points.

This phenomenon of sharp phase transition is observable in our applications, which we further explore through numerical experiments and display in Figure 7. Here, each curve corresponds to a numerical experiment. We also plot the corresponding connectivity of VR complexes with respect to the Euclidean distance

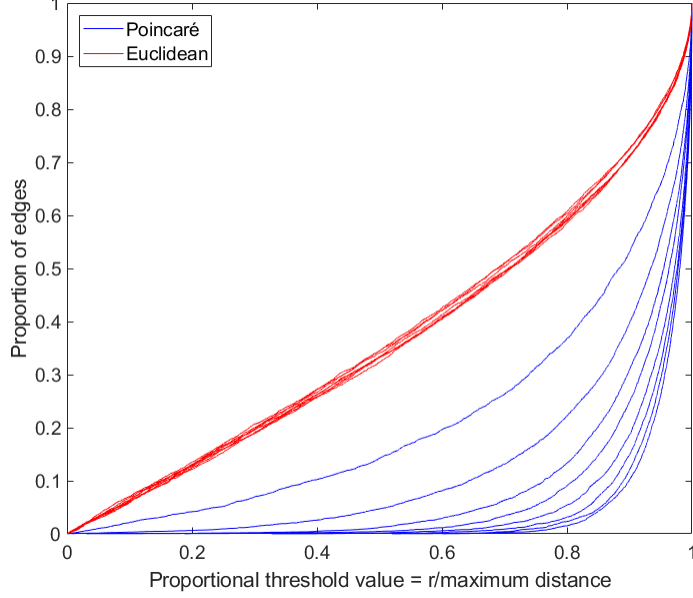


Figure 7: Cumulative distribution of edges Poincaré and Euclidean distances. Showing the proportion of edges in a VR filtration with respect to the Poincaré distance on the Poincaré ball (blue line) and the Euclidean distance on Euclidean space (red line), computed (9), against scaled VR threshold values Definition 2.

for comparison. For a given experiment, we draw the distance cumulative distribution function as follows: first, we normalize distances and sort them in ascending order; next, for the  $k$ th element  $R_k$ , we compute the proportion of connected pairs as

$$\frac{\#\{(x_i, x_j) \mid d_P(x_i, x_j) \leq R_k\}}{\#\{(x_i, x_j)\}}. \quad (9)$$

From the cumulative distribution plot in Figure 7, we see this rapidly increasing connectivity behavior at higher threshold values in repeated numerical experiments. In each experiment, points are sampled closer and closer to the boundary of the ball, and we see a progressively sharper jump in connectivity of the VR complex the closer to the boundary the points lie for the Poincaré distance. For the extreme case with points sampled closest to the boundary of the ball, when the VR threshold value is at 90% of the maximum distance, there are less than 10% pairs of points that are connected. This percentage sharply and dramatically increases at thresholds from 90% to the maximum distance, from 10% to 100% of pairs of points being connected. The phase change explains why we cannot see long persistence (in terms of points appearing far away from the diagonal) in dimension 1 or 2 in Figure 4. The connectivity of the VR complex under the Euclidean distance, in contrast, grows linearly with the threshold. Moreover, we see that the connectivity is stable and robust to the sampling location of the points since there is very little variability in the curves; the linear growth in connectivity is unaffected by the location of the sampled points.

Note that although the topology of the databases is not captured in the Poincaré ball embeddings, the dilation-invariant bottleneck distance for the ActivityNet embedding is nevertheless small, with a value of 0.5481 and corresponding dilation parameter value of 3.986. We do not see this coincidence for the Mammals dataset, however: the dilation-invariant bottleneck distances between the persistence diagram arising from the exponential map embedding and the direct Poincaré embedding remains large at 5.808 with a corresponding dilation parameter value of 3.182. This large dilation-invariant bottleneck distance is likely due to the difference in occurrences of homology between the two diagrams: the exponential map embedding picks up on spurious  $H_1$  and  $H_2$  homology, while the direct Poincaré embedding does not. There is no immediate interpretation for the dilation parameter value and its effect on the dilation-invariant bottleneck distances, due to the nonlinear and asymmetric behavior of the metric and derived approximations (see Figure 6).

Overall, we find that the higher-order connectivity and hierarchy of the databases was preserved in the Euclidean embeddings, but not in the Poincaré ball embeddings:  $H_1$  and  $H_2$  homology corresponding to cycles and voids appear in the persistence diagrams of the Euclidean embeddings, and do not in the Poincaré ball embeddings.

## 5 Discussion

In this work, we used persistent homology to quantify and study the topological structure of databases corresponding to their hierarchy and connectivity. We found that the Euclidean embeddings preserve the topology of the databases with respect to both the  $L_2$  and cosine similarity metrics, while the Poincaré ball embeddings did not. Moreover, we found that among topology-preserving embeddings, the topological structure captured by the persistence diagrams was consistent. To quantify this effect, we introduced the dilation-invariant bottleneck distance, which retains the similarity between persistence diagrams and erases the distortion effect of the different metrics over the embeddings. We found that dilation-invariant bottleneck distances between topology-preserving database representations are small.

Note that the goal of our work was to evaluate how different metric spaces maintain the topology of databases without any prior incentive to do so. This is in contrast to Moor et al. (2020) who explicitly enforce a topological constraint. Our motivation for doing so is with IR in mind: while “bad” databases may need their topology to be enforced, for “good” databases, this is not necessary. Our study is thus exploratory and in this work, we do not seek to improve the topological quality of the database representations. This work is the first step in assessing the utility of TDA as a viable tool in IR. Our findings show that without enforcing a topological prior, the topology is not preserved between two commonly-used embeddings to a high degree, which we quantify with the dilation-invariant bottleneck distance. Where the connectivity of the database is important, i.e., when we seek to preserve cycles and higher order topology, database embeddings into the Poincaré ball are less desirable. While embeddings into the Poincaré ball indeed preserve hierarchy and are useful when the databases are known to be trees, when it is *a priori* unknown if there exists a higher order structure that would be important for IR, our work shows that a more conservative approach would be to use an alternative embedding.

Our findings motivate the quantification of the added information and potential of increased accuracy in IR tasks when taking into account the topology of the hierarchy. This will entail the development of a new set of topological quality control and performance criteria, which will need to be interpretable in context and comparable to currently used methods. These criteria will need to be applied to both the queries submitted and the database, since queries are not always informative or well-designed, while databases may also suffer from missing or repeated entries and noise. An extensive set of experiments is required to assess all possible scenarios (i.e., for when queries are “bad,” but the database is “good,” and vice versa; and also when both the query and database are “bad.”). In future work, we aim to develop a topological criterion for preference of certain database embeddings over others, which may then be used to increase the precision of IR.

## Acknowledgments

A.M. thanks Henry Adams for helpful discussions.

## References

- Adams, H. and G. Carlsson (2015). Evasion paths in mobile sensor networks. *The International Journal of Robotics Research* 34(1), 90–104.
- Anderson, K. L., J. S. Anderson, S. Palande, and B. Wang (2018). Topological Data Analysis of Functional MRI Connectivity in Time and Space Domains. In G. Wu, I. Rekik, M. D. Schirmer, A. W. Chung, and B. Munsell (Eds.), *Connectomics in NeuroImaging*, Cham, pp. 67–77. Springer International Publishing.
- Aukerman, A., M. Carrière, C. Chen, K. Gardner, R. Rabadán, and R. Vanguri (2020). Persistent Homology Based Characterization of the Breast Cancer Immune Microenvironment: A Feasibility Study. In S. Cabello and D. Z. Chen (Eds.), *36th International Symposium on Computational Geometry (SoCG 2020)*, Volume 164 of *Leibniz International Proceedings in Informatics (LIPIcs)*, Dagstuhl, Germany, pp. 11:1–11:20. Schloss Dagstuhl–Leibniz-Zentrum für Informatik.
- Bauer, U. (2021, February). Ripser: efficient computation of Vietoris–Rips persistence barcodes. Preprint.
- Bevilacqua, M. and R. Navigli (2020). Breaking through the 80% glass ceiling: Raising the state of the art in word sense disambiguation by incorporating knowledge graph information. In *Proceedings of the 58th Annual Meeting of the Association for Computational Linguistics*, Online, pp. 2854–2864. Association for Computational Linguistics.
- Bobrowski, O., M. Kahle, and P. Skraba (2017, 08). Maximally persistent cycles in random geometric complexes. *Ann. Appl. Probab.* 27(4), 2032–2060.
- Boudin, F., Y. Gallina, and A. Aizawa (2020, July). Keyphrase generation for scientific document retrieval. In *Proceedings of the 58th Annual Meeting of the Association for Computational Linguistics*, Online, pp. 1118–1126. Association for Computational Linguistics.
- Brüel-Gabrielsson, R., B. J. Nelson, A. Dwaraknath, P. Skraba, L. J. Guibas, and G. Carlsson (2019). A Topology Layer for Machine Learning.
- Buchet, M., F. Chazal, S. Y. Oudot, and D. R. Sheehy (2016). Efficient and robust persistent homology for measures. *Computational Geometry* 58, 70–96.
- Carlsson, G. (2009). Topology and Data. *Bulletin of the American Mathematical Society* 46(2), 255–308.
- Chazal, F., D. Cohen-Steiner, L. J. Guibas, F. Mémoi, and S. Y. Oudot (2009). Gromov–Hausdorff Stable Signatures for Shapes using Persistence. *Computer Graphics Forum* 28(5), 1393–1403.
- Chazal, F., L. J. Guibas, S. Y. Oudot, and P. Skraba (2013). Persistence-Based Clustering in Riemannian Manifolds. *J. ACM* 60(6).
- Clementini, E., J. Sharma, and M. J. Egenhofer (1994). Modelling topological spatial relations: Strategies for query processing. *Computers & Graphics* 18(6), 815–822.
- Cohen-Steiner, D., H. Edelsbrunner, and J. Harer (2007). Stability of persistence diagrams. *Discrete & computational geometry* 37(1), 103–120.
- Crawford, L., A. Monod, A. X. Chen, S. Mukherjee, and R. Rabadán (2020). Predicting Clinical Outcomes in Glioblastoma: An Application of Topological and Functional Data Analysis. *Journal of the American Statistical Association* 115(531), 1139–1150.
- de Silva, V. and R. Ghrist (2006). Coordinate-free coverage in sensor networks with controlled boundaries via homology. *The International Journal of Robotics Research* 25(12), 1205–1222.
- Deolalikar, V. (2015, 01). Topological models of document-query sets in retrieval for enterprise information management. pp. 18–23.
- Edelsbrunner, H. and J. Harer (2008). Persistent Homology – a Survey. *Contemporary mathematics* 453, 257–282.

- Edelsbrunner, H., D. Letscher, and A. Zomorodian (2000). Topological persistence and simplification. In *Proceedings 41st Annual Symposium on Foundations of Computer Science*, pp. 454–463.
- Egghe, L. (1998). Properties of topologies of information retrieval systems. *Mathematical and Computer Modelling* 27(2), 61–79.
- Egghe, L. and R. Rousseau (1998). Topological aspects of information retrieval. *Journal of the American Society for Information Science* 49(13), 1144–1160.
- Everett, D. M. and S. C. Cater (1992a). Topology of document retrieval systems. *Journal of the American Society for Information Science* 43(10), 658–673.
- Everett, D. M. and S. C. Cater (1992b). Topology of document retrieval systems. *Journal of the American Society for Information Science* 43(10), 658–673.
- Frosini, P. and C. Landi (1999). Size theory as a topological tool for computer vision. *Pattern Recognition and Image Analysis* 9(4), 596–603.
- Ganea, O. E., G. Bécigneul, and T. Hofmann (2018). Hyperbolic neural networks. *Advances in Neural Information Processing Systems 2018(NeurIPS)*, 5345–5355.
- Ghrist, R. (2008). Barcodes: The persistent topology of data. *Bulletin of the American Mathematical Society* 45(1), 61–75.
- Google (2018). Kaggle Google Landmark Retrieval Challenge.
- Heilbron, F. C., V. Escorcia, B. Ghanem, and J. C. Niebles (2015). ActivityNet: A large-scale video benchmark for human activity understanding. In *Proceedings of the IEEE Conference on Computer Vision and Pattern Recognition*, pp. 961–970.
- Hiraoka, Y., T. Nakamura, A. Hirata, E. G. Escolar, K. Matsue, and Y. Nishiura (2016). Hierarchical structures of amorphous solids characterized by persistent homology. *Proceedings of the National Academy of Sciences*.
- Hirata, A., T. Wada, I. Obayashi, and Y. Hiraoka (2020). Structural changes during glass formation extracted by computational homology with machine learning. *Communications Materials* 1(1), 1–8.
- Hofer, C., R. Kwitt, M. Niethammer, and M. Dixit (2019). Connectivity-Optimized Representation Learning via Persistent Homology. In K. Chaudhuri and R. Salakhutdinov (Eds.), *Proceedings of the 36th International Conference on Machine Learning*, Volume 97 of *Proceedings of Machine Learning Research*, pp. 2751–2760. PMLR.
- Hofer, C., R. Kwitt, M. Niethammer, and A. Uhl (2017). Deep learning with topological signatures. *arXiv preprint arXiv:1707.04041*.
- Hu, X., L. Fuxin, D. Samaras, and C. Chen (2019). Topology-Preserving Deep Image Segmentation. pp. 1–11.
- Liu, J., X. Zhang, D. Goldwasser, and X. Wang (2020, December). Cross-lingual document retrieval with smooth learning. In *Proceedings of the 28th International Conference on Computational Linguistics*, Barcelona, Spain (Online), pp. 3616–3629. International Committee on Computational Linguistics.
- Long, T., P. Mettes, H. T. Shen, and C. G. M. Snoek (2020, June). Searching for actions on the hyperbole. In *Proceedings of the IEEE/CVF Conference on Computer Vision and Pattern Recognition (CVPR)*.
- Mathieu, E., C. L. Lan, C. J. Maddison, R. Tomioka, and Y. W. Teh (2019). Continuous Hierarchical Representations with Poincaré Variational Auto-Encoders.
- Miller, G. A. (1995). WordNet: A lexical database for english. *Commun. ACM* 38(11), 39–41.



- Moor, M., M. Horn, B. Rieck, and K. Borgwardt (2020). Topological Autoencoders. *Proceedings of the 37th International Conference on Machine Learning*, 1–18.
- Munkres, J. R. (2018). *Elements of algebraic topology*. CRC press.
- Nickel, M. and D. Kiela (2017). Poincaré embeddings for learning hierarchical representations. *Advances in Neural Information Processing Systems 2017*(NeurIPS), 6339–6348.
- Otter, N., M. A. Porter, U. Tillmann, P. Grindrod, and H. A. Harrington (2017). A roadmap for the computation of persistent homology. *EPJ Data Science* 6, 1–38.
- Patania, A., P. Selvaggi, M. Veronese, O. Dipasquale, P. Expert, and G. Petri (2019). Topological gene expression networks recapitulate brain anatomy and function. *Network Neuroscience* 3(3), 744–762.
- Perea, J. A. and G. Carlsson (2014). A Klein-Bottle-Based Dictionary for Texture Representation. *International journal of computer vision* 107(1), 75–97.
- Reininghaus, J., S. Huber, U. Bauer, and R. Kwitt (2015). A stable multi-scale kernel for topological machine learning. In *Proceedings of the IEEE conference on computer vision and pattern recognition*, pp. 4741–4748.
- Scarlini, B., T. Pasini, and R. Navigli (2020). SensEmBERT: Context-Enhanced Sense Embeddings for Multilingual Word Sense Disambiguation. In *Proceedings of the Thirty-Fourth Conference on Artificial Intelligence*, pp. 8758–8765. Association for the Advancement of Artificial Intelligence.
- Sheehy, D., O. Kisieliu, and N. J. Cavanna (2018). Computing the Shift-Invariant Bottleneck Distance for Persistence Diagrams. In *CCCG*, pp. 78–84.
- Tauzin, G., U. Lupo, L. Tunstall, J. B. Pérez, M. Caorsi, A. Medina-Mardones, A. Dassatti, and K. Hess (2020). giotto-tda: A topological data analysis toolkit for machine learning and data exploration.
- Yap, B. P., A. Koh, and E. S. Chng (2020, November). Adapting BERT for word sense disambiguation with gloss selection objective and example sentences. In *Findings of the Association for Computational Linguistics: EMNLP 2020*, Online, pp. 41–46. Association for Computational Linguistics.
- Zomorodian, A. and G. Carlsson (2005). Computing persistent homology. *Discrete & Computational Geometry* 33(2), 249–274.